Supplementary Files for

Machine learning models for outcome prediction of Chinese uveal melanoma patients: a 15-year follow-up study

Yu-Ning Chen[1†], Yi-Ning Wang[1†], Meng-Xi Chen[1†], Kai Zhang[2], Rong-Tian Chen[1], Rui Fang[1], Heng Wang[1], Hai-Han Zhang[1], Yi-Ning Huang[1], Yu Feng[1], Jing-Ting Luo[1], Yin-Jun Lan[1], Yue-Ming Liu[1*], Yang Li[1*], Wen-Bin Wei[1*]

[1]Beijing Tongren Eye Center, Beijing Key Laboratory of Intraocular Tumor Diagnosis and Treatment, Beijing Ophthalmology & Visual Sciences Key Lab, Medical Artificial Intelligence Research and Verification Key Laboratory of the Ministry of Industry and Information Technology, Beijing Tongren Hospital, Capital Medical University, Beijing, 100730, P. R. China

[2] InferVision Healthcare Science and Technology Limited Company, Shanghai, 200030, P. R. China

Table of Contents

Supplementary Materials and Methods

1. Study participants

This retrospective investigation included all patients treated for UM at the Beijing Tongren Eye Center (Beijing, China) between January 2005 and February 2020 (n = 1619). We excluded patients without complete clinical data (n = 40) and those who received treatment at other hospitals (n = 26). The remaining 1553 patients were evaluated and initially treated by our ophthalmological-oncologist team. These UM patients were included consecutively. The main diagnostic strategies were consistent with recommendations of the Collaborative Ocular Melanoma Study[1]. Demographic information (age, gender) and general ocular features (visual acuity, intraocular pressure, laterality) were recorded. Several strategies, including fundus photography, fluorescein angiography, indocyanine green angiography, standardized echography and orbital magnetic resonance imaging were conducted to assist diagnosis. Images and medical records were carefully evaluated for tumor-related features: tumor configuration, pigmentation, quadrant locations, optic disk involvement, association with subretinal fluid, intraocular hemorrhage, ciliary body involvement, and extraocular extension. The largest tumor basal diameter and thickness were measured using standardized ultrasonography. Extrascleral extension and ciliary body involvement were estimated based on thorough clinical checks and intraoperative findings. Tumors were staged according to the American Joint Committee on Cancer consensus (7^{th} edition)[2]. The type of therapy depended on the size and characteristics of the tumors, as described previously[3]. Histopathological examinations were available for patients who underwent local resection or enucleation. Tumor cell types were determined by light microscopy using hematoxylin-eosin staining. Time and sites of metastasis were documented. Time and cause of death were obtained from the patients' families. The survival time was defined as the interval (measured in months) between the date of the initial therapy or supportive care and the date of death or the date of the last follow-up (February 26, 2021).

2. Statistical analysis

Kaplan-Meier analysis was used to estimate survival and metastasis rate. For univariate

analysis, Chi-square tests were used, and we chose those variables with $P < 0.05$ as well as those with significant clinical features from previous studies[3, 4] (i.e., age, the largest tumor basal diameter and thickness) for multivariate analysis with Cox proportional hazard regression. The statistical analyses were performed using the Statistical Product and Service Solutions (SPSS) software version 25 (International Business Machines Corporation, Armonk, New York, United States).

3. Missing value completion

There were some missing data due to the loss of clinical data and some features that were not properly documented. The missForest algorithm (R package missForest, https://cran.r-project.org/web/packages/missForest/index.html) was used to impute missing values in the dataset[5]. MissForest iteratively filled all features with missing values by predicting missing values from existing values. The order for filling missing values was from features with the fewest missing values to the feature with the most missing values. Moreover, numerical features and nominal features were predicted with random forest regression and classification, respectively.

4. Prediction model

Machine learning is a powerful tool to mine hidden relationships in a dataset, including imaging, genetic, clinical, multimodal sensor data, and more[6-16]. Random forest[17, 18] was used to construct two models: whether a patient will survive for more than 2 years after treatment and whether the tumor will metastasize within 2 years of treatment using demographic attributes, general ocular features, and tumor-specific features. Some samples and features were excluded before constructing these two models as the dataset was preprocessed and then used to train the machine learning model.

Additionally, since all the datasets were imbalanced, we used a cost-sensitive matrix parameter, which is the most convenient manner for the random forest to address this type of problem. According to the algorithm mechanism, the random forest will resample the samples as the specific elements in a cost-sensitive matrix to form all sub-datasets in which the

minority will be resampled less than the majority to construct each decision tree. All the elements in the cost-sensitive matrix represent the cost for misclassifying a sample of class i to class j. The number of trees in the random forest was primarily set to 500 when experiments were carried out. Four-fold cross-validation was used to fairly evaluate the performance of random forest, and the subjects in each fold were independent[18]. We provided models in the format of .mat that can be applied repeatedly with MATLAB (https://github.com/Hugo0512/UM_Prognosis).

5. Feature selection

We applied the genetic feature selection to study which features were more informative in the two models. Then, all features selected by the genetic algorithm[19] were ranked with a feature ranking algorithm[18] to weigh their importance. To alleviate the stochasticity of the genetic algorithm and random forest, the genetic algorithm was repeatedly run 20 times and the run with the highest fitness function (classification accuracy) was chosen as the final result.

6. Evaluation metrics

Accuracy, sensitivity (recall rate), specificity, receiver operating characteristic curve (ROC), precision-recall (PR) curve and area under ROC curve [20, 21] were used to evaluate the performance of models. Mean value, standard deviation, and 95% confidence interval were evaluated for all metrics. ROC curve indicates how many samples of *i*th class are recognized conditioned on a specific number of *j*th class ($j \in [1,c]/i$), are classified as *i*th class, PR (precision-recall) curve illustrates how many samples of *j*th class are recognized as samples of *i*th class conditioned on a specific number of *j*th class ($j \in [1,c]/i$), are classified as *i*th class[21]. Precision is the ratio between the number of true positive and the total number of samples that were classified as positive. Accuracy, sensitivity (recall rate), specificity, precision were considered dimensionless.

References

1. Accuracy of diagnosis of choroidal melanomas in the Collaborative Ocular Melanoma Study. COMS report no. 1. Arch Ophthalmol. 1990;108(9):1268-73.

2. Shields CL, Kaliki S, Furuta M, Fulco E, Alarcon C, Shields JA. American Joint Committee on Cancer Classification of Uveal Melanoma (Anatomic Stage) Predicts Prognosis in 7,731 Patients: The 2013 Zimmerman Lecture. Ophthalmology. 2015;122(6):1180-1186.
3. Liu YM, Li Y, Wei WB, Xu X, Jonas JB. Clinical Characteristics of 582 Patients with Uveal Melanoma in China. PLoS One. 2015;10(12):e0144562.
4. Jager MJ, Shields CL, Cebulla CM, Abdel-Rahman MH, Grossniklaus HE, Stern MH, et al. Uveal melanoma. Nat Rev Dis Primers. 2020;6(1):24.
5. Lin D, Chen J, Lin Z, Li X, Zhang K, Wu X, et al. A practical model for the identification of congenital cataracts using machine learning. EBioMedicine. 2020;51:102621.
6. Kather JN, Pearson AT, Halama N, Jager D, Krause J, Loosen SH, et al. Deep learning can predict microsatellite instability directly from histology in gastrointestinal cancer. Nat Med. 2019;25(7):1054-6.
7. Mucaki EJ, Zhao JZL, Lizotte DJ, Rogan PK. Predicting responses to platin chemotherapy agents with biochemically-inspired machine learning. Signal Transduct Target Ther. 2019;4:1.
8. Wang L, Zhang K, Liu X, Long E, Jiang J, An Y, et al. Comparative analysis of image classification methods for automatic diagnosis of ophthalmic images. Sci Rep. 2017;7:41545.
9. Li W, Yang Y, Zhang K, Long E, He L, Zhang L, et al. Dense anatomical annotation of slit-lamp images improves the performance of deep learning for the diagnosis of ophthalmic disorders. Nat Biomed Eng. 2020;4(8):767-77.
10. Hannun AY, Rajpurkar P, Haghpanahi M, Tison GH, Bourn C, Turakhia MP, et al. Cardiologist-level arrhythmia detection and classification in ambulatory electrocardiograms using a deep neural network. Nat Med. 2019;25(1):65-9.
11. Liu Y, Jain A, Eng C, Way DH, Lee K, Bui P, et al. A deep learning system for differential diagnosis of skin diseases. Nat Med. 2020;26(6):900-8.
12. Mei X, Lee HC, Diao KY, Huang M, Lin B, Liu C, et al. Artificial intelligence-enabled rapid diagnosis of patients with COVID-19. Nat Med. 2020;26(8):1224-8.
13. Hyland SL, Faltys M, Huser M, Lyu X, Gumbsch T, Esteban C, et al. Early prediction of circulatory failure in the intensive care unit using machine learning. Nat Med. 2020;26(3):364-73.
14. Park SM, Won DD, Lee BJ, Escobedo D, Esteva A, Aalipour A, et al. A mountable toilet system for personalized health monitoring via the analysis of excreta. Nat Biomed Eng. 2020;4(6):624-35.
15. Yang J, Zhang K, Fan H, Huang Z, Xiang Y, Yang J, et al. Development and validation of deep learning algorithms for scoliosis screening using back images. Commun Biol. 2019;2:390.
16. Zhang Y, Li F, Yuan F, Zhang K, Huo L, Dong Z, et al. Diagnosing chronic atrophic gastritis by gastroscopy using artificial intelligence. Dig Liver Dis. 2020;52(5):566-72.
17. Zhang K, Liu X, Jiang J, Li W, Wang S, Liu L, et al. Prediction of postoperative complications of pediatric cataract patients using data mining. J Transl Med. 2019;17(1):2.
18. Zhang X, Zhang K, Lin D, Zhu Y, Chen C, He L, et al. Artificial intelligence deciphers codes for color and odor perceptions based on large-scale chemoinformatic data. Gigascience. 2020;9(2).
19. Zhang K, Pan Q, Yu D, Wang L, Liu Z, Li X, et al. Systemically modeling the relationship between climate change and wheat aphid abundance. Sci Total Environ. 2019;674:392-400.
20. Zhang K, Li X, He L, Guo C, Yang Y, Dong Z, et al. A human-in-the-loop deep learning paradigm for synergic visual evaluation in children. Neural Netw. 2020;122:163-73.
21. Zhang K, Liu X, Liu F, He L, Zhang L, Yang Y, et al. An Interpretable and Expandable Deep Learning Diagnostic System for Multiple Ocular Diseases: Qualitative Study. J Med Internet Res.

158 2018;20(11):e11144.
159

Supplementary Tables

Supplementary Table S1. Features of the 1553 UM patients' features, treatment, and outcome.

Feature	Category	Number of Patients (*n* = 1553 [%])
Demographic feature		
Gender	Male	793 (51.1%)
	Female	760 (48.9%)
Age (years)	≤ 20 years	20 (1.3%)
	21-40	439 (28.3%)
	41-60	861 (55.4%)
	61-80	231 (14.9%)
	> 80	2 (0.1%)
General ocular feature		
Laterality	Right	794 (51.1%)
	Left	759 (48.9%)
Visual acuity (LogMAR) (available for 1507 patients)	> 1.00	512 (34.0%)
	0.31-1.00	527 (35.0%)
	0.10-0.30	234 (15.5%)
	≤ 0.10	234 (15.5%)
Intraocular pressure (mmHg) (available for 1494 patients)	< 10	148 (9.9%)
	10-21	1279 (85.6%)
	> 21	67 (4.5%)
Tumor-specific features		
Size (AJCC Classification) (available for 1530 patients)	T1	219 (14.3%)
	T2	619 (40.5%)
	T3	564 (36.9%)
	T4	128 (8.4%)
Pigmentation	Pigmented	1538 (99.0%)
	Non-pigmented	15 (1.0%)
Location of tumor in uveal melanoma	Ciliary body	66 (4.2%)
	Iris	5 (0.3%)
	Choroid	1482 (95.4%)
Position (available for 1522 patients)	Superior	114 (7.5%)
	Nasal	164 (10.8%)
	Inferior	105 (6.9%)
	Temporal	279 (18.3%)
	Superior temporal	298 (19.6%)
	Superior nasal	117 (7.7%)
	Inferior nasal	124 (8.1%)
	Inferior temporal	257 (16.9%)
	Macula	58 (3.8%)
	Bifocal	6 (0.4%)
Macroscopic appearance (available for 1411 patients)	Mushroom	481 (34.1%)
	Flat	87 (6.2%)
	Hemisphere	710 (50.3%)
	Irregular	114 (8.1%)
	Diffuse	19 (1.3%)
Optic disk involvement	Yes	74 (4.8%)
	No	1479 (95.2%)
Subretinal fluid (available for 1541 patients)	Yes	1154 (74.9%)
	No	387 (25.1%)

Intraocular hemorrhage (available for 1524 patients)	Yes	77 (5.1%)
	No	1447 (94.9%)
Ciliary body involvement (available for 1552 patients)	Yes	235 (15.1%)
	No	1317 (84.9%)
Extraocular extension	Yes	11 (0.7%)
	No	1542 (99.3%)
T stage* (available for 1530 patients)	T1a	198 (12.9%)
	T1b	21 (1.4%)
	T2a	588 (38.4%)
	T2b	29 (1.9%)
	T2c	1 (0.1%)
	T2d	1 (0.1%)
	T3a	451 (29.5%)
	T3b	109 (7.1%)
	T3c	2 (0.1%)
	T3d	2 (0.1%)
	T4a	55 (3.6%)
	T4b	68 (4.4%)
	T4c	3 (0.2%)
	T4d	2 (0.1%)
M stage* (available for 1530 patients)	M0	1530 (100.0%)
TNM stage* (available for 1530 patients)	I	198 (12.9%)
	IIA	609 (39.8%)
	IIB	480 (31.4%)
	IIIA	168 (11.0%)
	IIIB	73 (4.8%)
	IIIC	2 (0.1%)
Initial treatment	Episcleral brachytherapy	1122 (72.2%)
	Local resection	74 (4.8%)
	Enucleation	234 (15.1%)
	Local laser phototherapy	112 (7.2%)
	Observation or refuse treatment	11 (0.7%)
Pathology (available for 386 patients)	Spindle cell-type	172 (44.6%)
	Epithelioid cell-type	83 (21.5%)
	Mixed cell-type	131 (33.9%)
Outcome	Living without metastasis	1292 (83.2%)
	Metastasis	237 (15.3%)
	Death	210 (13.5%)
Follow-up time (years)	≤ 1	176 (11.3%)
	> 1 and ≤ 3	486 (31.3%)
	> 3 and ≤ 5	386 (24.9%)
	> 5 and ≤ 10	456 (29.4%)
	> 10	49(3.2%)

163 * American Joint Committee on Cancer classification (7th edition)

164 Abbreviations: *UM: Uveal Melanoma; LogMAR: Logarithm of the Minimum Angle of*

165 *Resolution; AJCC: American Joint Committee on Cancer; TNM: Tumor Node Metastasis*

Supplementary Table S2. Sites of metastasis

Patients with metastasis	Metastatic sites												
	Liver	Lung	Breast	Bone	Ovary	Brain	Abdomen	Lymph	Spleen	Skin	Pancreas	Orbit	Stomach
No. (n = 225)	201	54	3	40	1	17	3	4	1	2	2	7	1
%	89.3	24.0	1.3	17.8	0.4	7.6	1.3	1.8	0.4	0.9	0.9	3.1	0.4

Supplementary Table S3. Univariate analysis by Kaplan-Meier and multivariate analysis by Cox regression for UM-related metastasis and all causes of death.

Features	1553 cases	UM-related metastasis (237 patients)					All-causes death (210 patients)				
		Univariate analysis		Multivariate analysis			Univariate analysis		Multivariate analysis		
	n/Mean	Chi-square	*P*	*P*	HR	95% CI	Chi-square	*P*	*P*	HR	95% CI
Gender		0.091	0.763				0.495	0.482			
Male	793										
Female	760										
Age (years)		7.563	**0.006**				24.427	**<0.001**			
≤ 56	1219			Ref	-	-			Ref	-	-
> 56	334			**<0.001**	1.814	1.305-2.520			**<0.001**	2.426	1.725-3.410
Laterality		0.387	0.534				0.143	0.705			
Right	794										
Left	759										
Visual acuity (LogMAR)		12.982	**0.005**	0.249			8.421	**0.038**	0.994		
> 1.00	512			0.359	0.810	0.516-1.271			0.929	0.976	0.576-1.655
0.31-1.00	527			0.282	0.786	0.507-1.219			0.941	0.981	0.590-1.632
0.10-0.30	234			0.044	0.555	0.313-0.984			0.895	1.041	0.575-1.884
≤ 0.10	234			Ref	-	-			Ref	-	-
Intraocular pressure (mmHg)		6.798	**0.033**	0.346			4.843	0.089			
< 10	148			0.310	1.242	0.817-					

10-21	1279			Ref	-	1.888 -					
> 21	67			0.256	1.571	0.721-3.423					
Largest basal diameter (mm)	11.70	565.199	**<0.001**	**<0.001**	1.223	1.123-1.332	366.774	**<0.001**	**<0.001**	1.199	1.093-1.314
Thickness (mm)	6.90	354.315	**<0.001**	0.678	0.980	0.892-1.077	395.124	**<0.001**	0.533	0.969	0.876-1.071
Size		71.722	**<0.001**	0.331			64.691	**<0.001**	0.487		
T1	219			Ref	-	-			Ref	-	-
T2	619			0.311	0.258	0.019-3.556			0.326	0.269	0.020-3.687
T3	564			0.674	0.372	0.004-37.387			0.664	0.358	0.004-36.522
T4	128			0.573	0.156	<0.001-99.241			0.676	0.250	<0.001-167.513
Pigmentation		0.811	0.368				3.772	**0.052**			
Pigmented	1538								Ref	-	-
Non-pigmented	15								**0.031**	3.693	1.123-12.144
Location		2.318	0.314				4.964	0.084			
Ciliary body	66										
Iris	5										
Choroid	1482										
Position		9.970	0.353				19.763	**0.019**	**0.033**		
Superior	114								Ref	-	-
Nasal	164								0.797	0.902	0.410-1.984
Inferior	105								0.957	0.977	0.415-2.302
Temporal	279								0.541	0.811	0.414-1.588
Superior temporal	298								0.289	1.416	0.745-2.691
Superior nasal	117								0.143	1.713	0.834-3.516
Inferior nasal	124								0.812	1.095	0.519-2.312
Inferior temporal	257								0.888	1.049	0.5433-2.025
Macula	58								0.493	1.622	0.407-6.457
Bifocal	6								**0.004**	7.383	1.912-28.514
Macroscopic appearance		77.301	**<0.001**	**<0.001**			45.967	**<0.001**	**0.011**		
Mushroom	481			**0.003**	0.420	0.238-			0.087	0.581	0.312-1.082

Flat	87			0.114	0.345	0.741 0.092-1.292			0.133	0.356	0.093-1.369
Hemisphere	710			**<0.001**	0.401	0.271-0.595			**0.002**	0.476	0.301-0.753
Irregular	114			Ref	-	-			Ref	-	-
Diffuse	19			0.543	1.489	0.413-5.364			0.562	1.472	0.399-5.439
Optic disk involvement		2.715	0.099				1.624	0.203			
Yes	74										
No	1479										
Subretinal fluid		38.747	**<0.001**				21.352	**<0.001**			
Yes	1154			**<0.001**	2.491	1.541-4.027			**0.039**	1.603	1.024-2.507
No	387			Ref	-	-			Ref	-	-
Intraocular hemorrhage		2.118	0.146				0.972	0.324			
Yes	77										
No	1447										
Ciliary body involvement		21.970	**<0.001**				20.126	**<0.001**			
Yes	235			0.954	1.063	0.132-8.558			0.971	1.040	0.125-8.618
No	1317			Ref	-	-			Ref	-	-
Extraocular extension		1.149	0.284				1.954	0.162			
Yes	11										
No	1542										
TNM stage		76.879	**<0.001**	0.625			68.794	**<0.001**	0.745		
I	198			Ref	-	-			Ref	-	-
IIA	609			0.234	5.118	0.347-75.517			0.303	4.054	0.283-58.090
IIB	480			0.592	3.507	0.036-343.705			0.580	3.655	0.037-359.090
IIIA	168			0.614	5.216	0.008-3210.984			0.623	5.026	0.008-3162.337
IIIB	73			0.664	6.360	0.002-26769.696			0.716	4.764	0.001-21496.515

IIIC	2			0.990	<0.001	<0.001-			0.987	<0.001	<0.001-
Initial treatment		19.681	**0.001**	0.364			16.895	**0.002**	0.731		
Episcleral brachytherapy	1122			Ref	-	-			Ref	-	-
Local resection	74			0.939	<0.001	<0.001-			0.184	0.246	0.031-1.950
Enucleation	234			0.181	0.675	0.380-1.200			0.701	0.886	0.478-1.643
Local laser phototherapy	112			0.668	1.224	0.486-3.086			0.630	0.770	0.267-2.224
Observation or refuse treatment	11			0.118	4.931	0.665-36.537			0.959	<0.001	<0.001-
Pathology		14.204	**0.001**				14.712	**0.001**			
Spindle cell-type	172										
Epithelioid cell-type	83										
Mixed cell-type	131										

Abbreviations:

UM: Uveal Melanoma

LogMAR: Logarithm of the Minimum Angle of Resolution

TNM: Tumor Node Metastasis

Supplementary Table S4. Four-fold cross-validation result for predicting death.

Metrics	All features	Feature selection
Accuracy	0.7696(0.0358)/ [0.6994 0.8398]	0.8929 (0.0053)/ [0.8825 0.9033]
Sensitivity	0.7665 (0.0370)/ [0.6940 0.8390]	0.8913 (0.0055)/ [0.8805 0.9022]
Specificity	0.8393 (0.1072)/ [0.6293 1.0000]	0.9286 (0)/ [0.9286 0.9286]
AUC	0.8839 (0.0442)/ [0.7974 0.9704]	0.9264 (0.0078)/ [0.9112 0.9417]

The values in the table are "Mean (Standard Deviation) / [95% Confidence Interval]", respectively.

Abbreviations:

AUC: Area Under Curve

Supplementary Table S5. Four-fold cross-validation result for predicting metastasis.

Metrics	All features	Feature selection
Accuracy	0.7495 (0.0244)/ [0.7017 0.7974]	0.6946 (0.0134)/ [0.6683 0.7208]
Sensitivity	0.7467 (0.1131)/ [0.5249 0.9684]	0.9092 (0.0682)/ [0.7756 1.0000]
Specificity	0.7498 (0.0290)/ [0.6929 0.8066]	0.6767 (0.0189)/ [0.6396 0.7138]
AUC	0.8466 (0.0397)/ [0.7688 0.9244]	0.8714 (0.0354)/ [0.8021 0.9407]

The values in the table are "Mean (Standard Deviation) / [95% Confidence Interval]", respectively.

Abbreviations: AUC: Area Under Curve

Supplementary Figures

Supplementary Figure S1. Six factors related to death according to multivariate analysis.

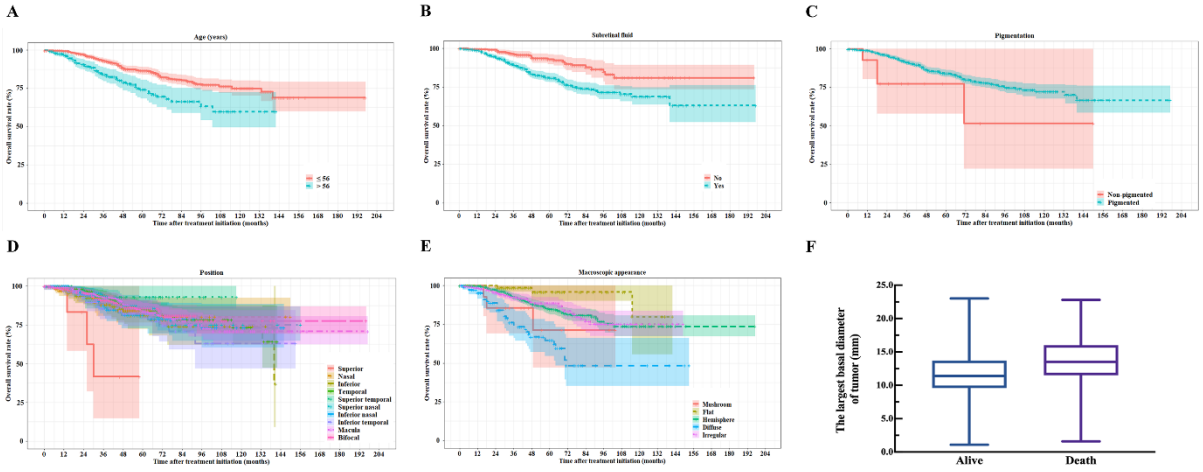

(A) Kaplan-Meier graph of age. **(B)** Kaplan-Meier graph of subretinal fluid. **(C)** Kaplan-Meier graph of tumor pigmentation. **(D)** Kaplan-Meier graph of tumor position. **(E)** Kaplan-Meier graph of tumor's macroscopic appearance. **(F)** Boxplot of the largest tumor basal diameter by patients' survival state. The line in the box indicated the median, the box indicated the interquartile range, and the top and bottom lines represented the maximum and minimum values.

Supplementary Figure S2. Four factors related to metastasis according to multivariate analysis

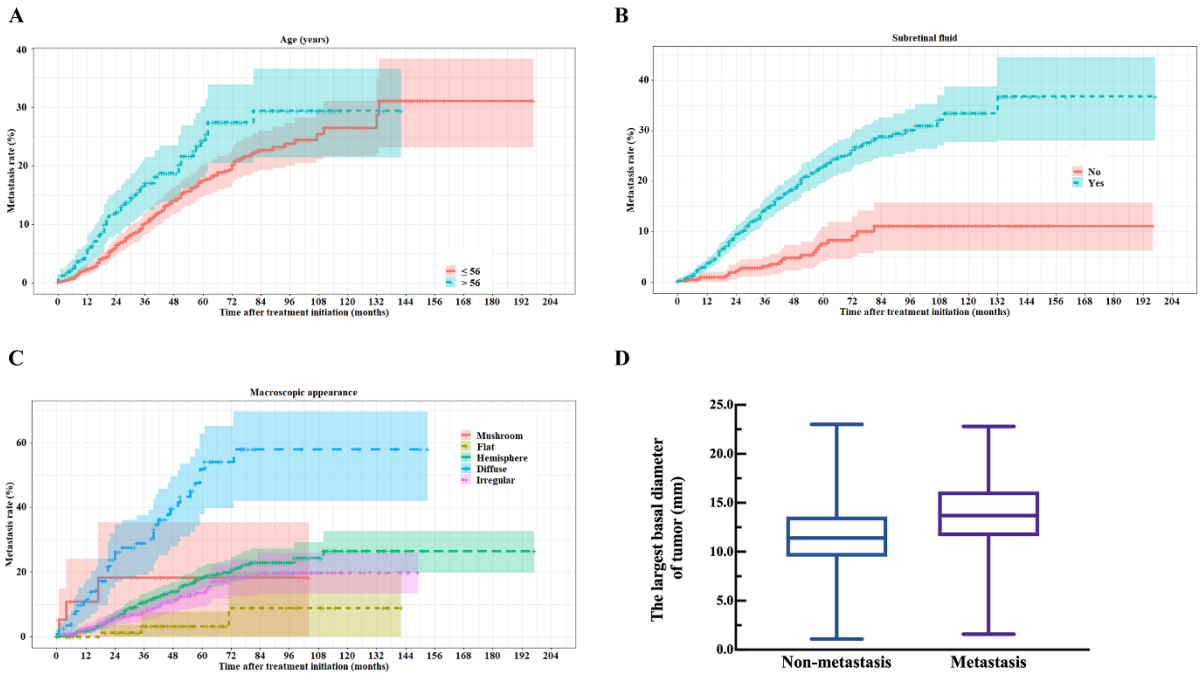

(A) Kaplan-Meier graph of age. (B) Kaplan-Meier graph of subretinal fluid. (C) Kaplan-Meier graph

of tumor's macroscopic appearance. (D) Boxplot of the largest tumor basal diameter by patients' metastasis state. The line in the box indicated the median, the box indicated the interquartile range, and the top and bottom lines represented the maximum and minimum values.

Supplementary Figure S3. Machine learning result of death model (UMDeath)

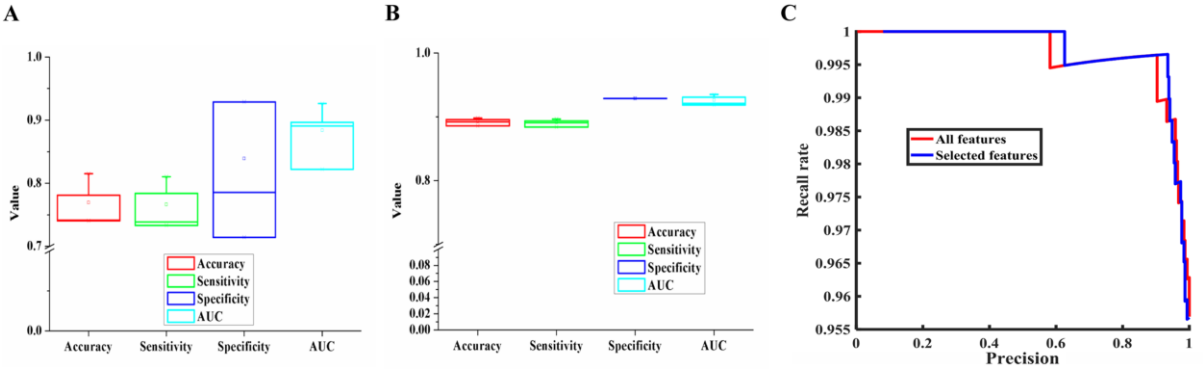

(A) Boxplot of four-fold cross-validation results of all metrics for the predictive results with all features. The line in the box indicated the median, the box indicated the interquartile range, and the top and bottom lines and asterisks represented the 1% and 99% percentiles. The little box indicated the mean value. **(B)** Boxplot of four-fold cross-validation results of all metrics for the predictive results with selected features. **(C)** PR curve of predicting model for death after two years of treatment.

Abbreviations: PR: Precision-Recall, AUC: Area Under Curve

Supplementary Figure S4. Machine learning result of metastasis model (UMMetastasis)

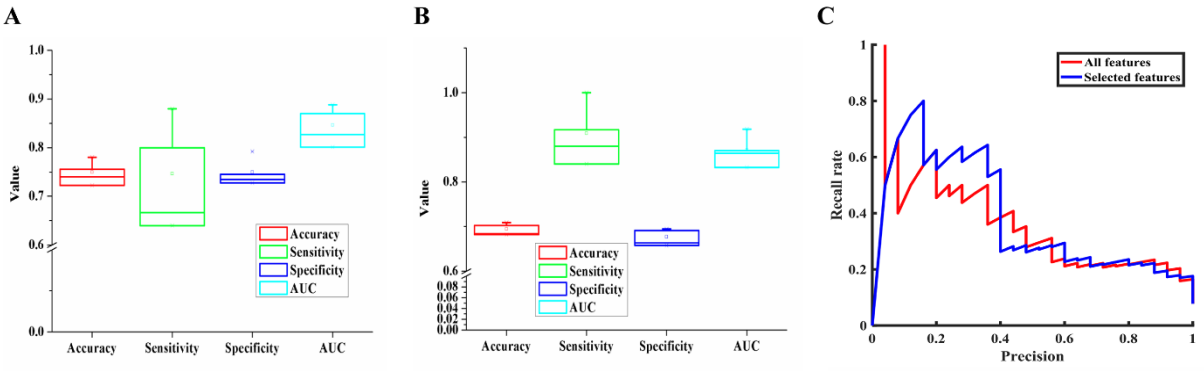

(A) Boxplot of four-fold cross-validation results of all metrics for the predictive results with all features. The line in the box indicated the median, the box indicated the interquartile range, and the top and bottom lines and asterisks represented the 1% and 99% percentiles. The little box indicated the mean value. **(B)** Boxplot of four-fold cross-validation results of all metrics for the predictive results with selected features.

(C) PR curve of predicting model for metastasis within two years of treatment.

Abbreviations: PR: Precision-Recall, AUC: Area Under Curve